Proceedings of the Korean Nuclear Society Spring Meeting
Gyeongju, Korea, May 2003

A Study on the Effect of Various Spacer Grids on CHF in 2*2 Rod Bundle with R-134a

Byung Soo Shin, Soon Heung Chang

Korea Advanced Institute of Science and Technology
373-1, Guseong-dong, Yuseong-gu, Daejeon, Korea, 305-701

Abstract

Experimental investigation was performed using the 2*2 rod bundle in order to find out the effect of spacer grid on CHF with R-134a. The rod diameter of test section is 9.7mm. Rod pitch is 12.95mm. An outside-line of flow channel is 25.7mm. As test spacer grids, three different types of spacer grid that was applied for a patent by KAERI and *V-5H* were selected. Experimental conditions are as follows: Mass flux is from 1000 to 1800 kg/m^{2}s, inlet temperature is from 10 to 20^{o}C, and inlet pressure is 20 bar.

Flow structure experiment was also performed with single-phase water at room temperature and atmospheric pressure. The result of CHF experiment was explained through this experiment qualitatively. In this experiment, using LDV, we measured axial and lateral velocity and turbulent intensity along the centerline to find out the swirl magnitude and turbulent kinetic energy. And using DP cell, pressure drop was also measured.

Consequently, the swirl flow and turbulent level forming by spacer grid and mixing vane contributed to the CHF enhancement. The ratio of enhancement was changed as the distance from spacer grid. And we also confirmed that a blockage area was an important parameter in view of pressure drop.

1. Introduction

CHF phenomena means that as flow condition or heating condition is changed, heat transfer coefficient near the heating wall decrease suddenly in boiling heat transfer system. CHF phenomena are classified to two mechanisms on flow rate and pressure: LFD (liquid film dryout) and DNB (departure of nuclear boiling). To explain the physical mechanism of DNB, there are two well-known models. One is “Bubble Crowding Model” proposed by Weisman & Pei, The other is “Liquid Sublayer Dryout Model” proposed by Lee & Mudawwar. The former tells that when wall void fraction is over a specific value, CHF occurs. The latter tells that when liquid sublayer near the wall is evaporated, CHF occurs.

Since CHF phenomena limit thermal-hydraulic performance in various heat transfer system and nuclear power plant, it is a meaningful to enhance the CHF magnitude. Many researchers have investigated on method of CHF enhancement. Specially, many methods of CHF enhancement were proposed in circular tube: For example, the insertion of twisted tape, variations of surface roughness, use of ribbed tube and etc. From these methods, we can expect the effect like these: (i) to supply liquid to wall (ii) turbulent increase (iii) to break a large bubble. In nuclear power plant, to enhance the CHF value, spacer grid and mixing vane are adopted. A basic role of spacer grid is to support the interval between rods. In thermal hydraulic viewpoint, Spacer grid and mixing vane change flow structure and, therefore, enhance the CHF value but increase the pressure drop as a flow obstacle.

When flows pass through the spacer grid, three additional flows are generated like these: (i) swirl flow, (ii) cross flow, (iii) turbulent mixing. We know that in DNB region, these factors enhance the CHF according to many researches. Therefore shape and characteristic of spacer grid and mixing vane is relative to CHF enhancement.

Major features of turbulent phenomena in subchannels include swirl flow, cross-flow mixing between subchannels and anisotropy of turbulent diffusion. It was illustrated in Fig.2.1. Several researchers have studied that the flow structure and characteristics near spacer grids in rod bundles. (Karoutas et al [1], Yue Fen Shen et al [2], Sun Kyu Yang et al [3] and Wang Kee In et al [4])

Karoutas et al [1] had studied the flow dynamics of spacer grids using CFD code and LDV. They measured the axial velocity and lateral velocity along the centerline in the 5*5 rod bundle. Test spacer grids were CE-type spacer grid with split vane and spacer grid with squeezed tube. They defined and calculated swirl factor. From the viewpoint of swirl factor, CFD-code predicted the actual phenomena well.

Yue Fen Shen et al [2] investigated a crossflow mixing effect caused by spacer grid with ripped-open mixing blades in a 4*4 rod bundle. Using an LDV, detailed measurements were performed with water to obtain information on the distributions of transverse mean velocity and RMS velocity for the flow through a 4*4 rod bundle on spacer grid with the mixing blades at various blade angles. They concluded that the mixing rate depends on the angle of the blade. They also proposed that the best angle of blade is 25^{o}, and the worst is 35^{o}.

Sun Kyu Yang et al [3] studied on the spacer grid effect on turbulent flow structure by using an LDV in subchannels of 5*5 rod bundle with spacer grids. The measured parameters are axial velocity, turbulent intensity, skewness factor and flatness factor. Pressure drop is measured, too. From these data, it was found that the turbulent mixing and forced mixing occur up to x/D_h=10 and 20 from the spacer grid, respectively.

Wang Kee In et al [4] performed CFD analysis to propose the optimized design of mixing vane on the spacer grid in a PWR fuel assembly. The considered mixing vanes are split vane, swirl-vane and twisted vane. From CFD analysis, the mixing effect by swirling flow and cross-flow, turbulent mixing and pressure drop were estimated and compared for the various vane angles. The optimized vane angle is proposed to be 40 and 35 from the axial-axis.

Many researchers have investigated the effect of spacer grid on the CHF. Generally the spacer grids increase the CHF. According to the experimental results of Rosal et al [13], mixing vane grid gave highest CHF, up to 26% higher than bundles not equipped with grid spacers. The experimental ranges were followings, pressure: 1490-2400psia; inlet temperature: 431-627^{o}F; and mass velocity: 1.02-3.95*10^{6} lb/hrft^{2}. The 284 DNB data points

obtained were compared with DNB heat fluxes predicted by the non-uniform heat flux W-3 correlation with a grid factor, based on local conditions calculated by the THINC computer code.

GUO Zhongchuan et al [8] investigated on the effect of mixing vane on CHF. They used three spacer grids: simple support grids, mixing vane grids and the grids with both mixing and guide vanes. They concluded that the mixing vanes can increase CHF value under subcooling and low quality conditions, and the guide vanes decrease the blocking effect at upstream of the spacer and increase the under high quality conditions.

Mixing vanes are not only effective to the CHF magnitude but also CHF locations. The study on this was performed by F. de Crecy [6] in 1994. His experimental studies were carried out on electrically heated, 5*5 square pitched, vertical rod bundles. He concluded that with mixing vanes, DNB occur on any of the nine central rods and is distributed in an apparently random way around the rod.

Cheng et al [11] studied on the CHF and turbulent mixing in hexagonal tight rod bundles. Especially, the effect of various parameters on CHF has been analyzed. It was found that the two-phase mixing coefficient depends mainly on mass flux. At the same time, the CHF in the tight rod bundle is much lower than that in a circular tube of the same equivalent hydraulic diameters. And the effect of wire wraps on CHF is mainly dependent on local vapor qualities and subsequently on flow regimes. Table 1.1 summarizes various experiments on the effect of spacer grid and mixing vane.

This study provides CHF experimental results with various spacer grids in 2*2 rod bundle with R-134a. The locations of spacer grids are 9cm and 18cm from the upper end of heated rod. Also, we measure the velocity profiles and velocity fluctuations along the centerline of subchannel in the water loop with LDV system. From this measurement, swirl magnitude and turbulent mixing are calculated. Here, our goals are to identify the relation between the CHF enhancements and flow structure and to find out effective parameters on the pressure drop.

2. Experiments

2.1 Test spacer grid

In this study, four different spacer grids are used. The characteristics are summarized in Table 2.1. These spacer grids were designed and applied for a patent by KAERI except one, *Vantage-5H*. *Vantage-5H* is the spacer grid for 17*17 nuclear fuel assembly designed by Westinghouse. When spacer grids were manufactured for 2*2 geometry, the blades bent toward the outside were cut but the rest blades were left. Fig.2.1 shows configurations of spacer grids. The comments for *V-5H* are omitted because it is a very popular spacer grid. For *two-strap spacer grid*, the main characteristic is that there are nozzles under the blade. In this spacer grid, we can expect that the swirl flow increase from injection of a part of flow to the blade by force. *Hybrid spacer grid* has both merits of split vane and these of swirl vane. Its mixing vane is composed of two main blades and two assistant blades. Therefore we can expect the increment of the cross flow as well as swirl flow. Finally, *swirl spacer grid* has typical swirl blades. We expect this spacer grid induces swirl flow.

2.2 CHF experiments

The Experimental loop is a closed circulation loop with R-134a as a working fluid. The loop has a test section, a condenser, a pump, a chiller, a preheater, an accumulator, valves, and instrumentations. The vacuum pump is also provided because air in the test section should be removed after the replacement of spacer grid. The loop is schematically shown in Fig.2.2. Almost all pipes of the loop are made of 1" SUS 316 tube to prevent corrosion. But pipes for measurements are 1/4" SUS 316 tube.

The main goal of this loop is to control the test section inlet conditions: inlet pressure, inlet temperature, and mass flux. Because R-134a is a compressible liquid, Pressure is coupled with temperature. So it is hard to control these inlet conditions. The components, which control pressure and temperature, are condenser, chiller, accumulator and preheater. Condenser made two-phase flow into single-phase flow. Together with chiller, condenser removes of heat from the working fluid at the test section outlet. Especially, it effect on the inlet pressure. Of course, the main role of condenser is a phase change. On the other hand, that of chiller is a heat removal. Accumulator simply controls the pressure of the loop. Inside accumulator, there is a membrane between N_2 gas and R-134a and pressure is dependent in amount of N_2 gas. Preheater is a component that controls the inlet subcooling (inlet temperature).

Test section's geometry is a 2*2 rod bundle. It composed of heater rod, copper plate for electrical connection, Bakelite for insulation, SUS 304 circular body. Fig 2.3 shows the structure of test section. Heater rod diameter is 9.7mm and the pitch is 12.85mm and a side of rectangular flow channel is 25.7mm and heated length is 1200mm. Each rod has a hole. Thermocouples (Type-K) are welded onto the inner surface of the rod at the upper end of heated length. Heater rod is shown in Fig 2.4.

200kW (40 V, 5000 A), direct current (DC) power supply system is used to provide direct joule heating of the stainless steel heater rod. The resistance of a heater rod is calculated as follows.

$$R = \rho \frac{L}{A} = \left(72\times10^{-8}\right)\times\frac{1.2}{\left(\left(9.7\times10^{-3}\right)^2-\left(9.1\times10^{-3}\right)^2\right)\times(\pi/4)} \qquad (3\text{-}1)$$

But the resistivity of heater rod increase as the temperature increases. So, this value must be determined by measurement.

Spacer grid without mixing vane (simply supported) is located at 600mm bottom from the location of test spacer grid. This interval is always fixed. Then, test spacer grid is located at 90mm or 180mm from the upper end of heater rod.

Table 2.2 shows test conditions of present experiments. According to Ahmad's scaling law [16], the conditions are correspond to following scales; pressure is about 6 times, mass flux is 1.2 times, heat flux is 11.63 times compared to water.

For bare (no spacer grid), full set will be performed, but for the space grids, the experiment will be performed only at 20bar.

2.3 Flow structure experiments

The test section's geometry of this experiment is the same as the CHF experiment. But the structure of this test section is simpler than that of CHF test, because this is non-heating experiment. The material is acryl for LDV measurement. And fully developed length is determined from Equation (3-2).

$$Z = 25 \sim 40 D_e \qquad (3\text{-}2)$$

The upper length is determined from the location of spacer grid in the CHF experiment. This is 250mm. This is shown in Fig 2.5. In this experiment, working fluid is single-phase water and mass flux is 1470kg/m^{2}s. Pressure and temperature is atmospheric pressure and room temperature.

Axial and radial velocity profiles are measured along the centerline at the cross section and the turbulent intensities are also measured. The locations of the cross section are shown in Fig 2.6.These are 5mm, 30mm, 60mm, 90mm(or 85mm for "Hybrid"), 128mm(or 123mm for "Hybrid"), 150mm and 180mm from the end of the mixing blade. Then, at each cross section, the measured points are marked in Fig 2.7.The interval of measured points is 1mm. And the velocities and turbulent intensities are measured from –5mm to 5mm along the centerline (11 points).

2.4 Estimation factors

From the result of the flow structure experiment, we need to estimate the effects of each spacer grid on the flow characteristics quantitatively. There are three considerations: swirl flow, cross flow, turbulent intensity. In this study we can examine two considerations except cross flow due to a subchannel. From previous researchers, some mathematical expressions have been proposed as follows.

Swirl Flow

The Swirl Factor: The integration of the absolute lateral velocity along the centerline in the lateral directions

$$F_{SW} = \frac{1}{2p}\int \frac{|V_{lateral}|}{V_{bulk}} dl \qquad (3\text{-}3)$$

The Swirl-Mixing Angular Momentum Flux Ratio

$$S_{AM} = \frac{\int r|V_\theta V_{axial}|dA}{R_S \int V_{axial}^2 dA} \qquad (3\text{-}4)$$

The Swirl-Mixing Kinetic Energy Ratio: The ratio of lateral kinetic energy to axial kinetic energy

$$S_{KE} = \frac{\int V_{lateral}^2 dA}{\int V_{axail}^2 dA} \qquad (3\text{-}5)$$

Cross Flow

The Cross Mixing Flow

$$F_{CM} = \frac{1}{S}\int \frac{|V_{cross}|}{V_{bulk}} dy \qquad (3\text{-}6)$$

Turbulent Intensity

Area-Averaged Turbulent Kinetic Energy Ratio

$$F_{KE} = \frac{1}{A}\int \left(\kappa / V_{bulk}^2\right) dA \qquad (3\text{-}7)$$

3. Results and Discussions

3.1 CHF Variations by Various Spacer Grids and Mixing Vanes

3.1.1 CHF Magnitude

Generally CHF phenomenon occurs when the local conditions, for example like wall void fraction, are over some critical point. The local conditions change according to the flow state, heat flux, geometry and working fluid. To express the relationship between the CHF and conditions, there are three well-known hypotheses: local conditions hypothesis, inlet conditions hypothesis, and outlet condition hypothesis. This study was performed with inlet conditions hypothesis.

Fig.3.1 shows the CHF variations with inlet conditions for the bare test section. The results coincide to the general trend. When the pressure and geometry are constant, Mass flux is positive effect and inlet temperature (negative inlet subcooling) is negative effect on the CHF. And the slope is almost same at any mass flux. This graph is used as a reference to the CHF experiment with spacer grid.

3.1.2 Spacer Grid Shape Effect

From Fig.3.2 to Fig.3.7, CHF variations are shown with the various spacer grids. These results classified to two kinds according to the location of spacer grid: 90mm and 180mm. The descriptions of former are Fig.3.2-Fig.3.4 and these of the latter are Fig.3.5-Fig.3.7. Here, we discuss about the case of 180mm, because in this case CHF difference between spacer grids is clearly observed.

Four types of spacer grid are used. The characteristic of each spacer grid was mentioned at the experimental work. We defined enhancement power ratio for the quantitative comparison of the effects of spacer grid on CHF represented as follow.

$$EPR = \frac{q''_{sp} - q''_{bare}}{q''_{bare}} \times 100(\%) \qquad (4\text{-}1)$$

In this study, EPR was calculated at center points of the line to fit each curve linearly. That is, this value represents average value of each curve. In Table 3.1 and Table 3.2, the calculated value is summarized.

In Table 3.2 and Figure 3.5-3.7, spacer grids increase CHF magnitude. But the EPRs of one spacer grid are not same as others and vary from 5.53% to 15.62%. Here, *swirl type spacer grid* has a best performance in view of EPR. And the following is that *hybrid spacer grid* and *V-5H* compete with each other. Finally, *two-strap spacer grid* is a worst. Strictly speaking, the priority order has some trend except the condition at which spacer grid location is 180mm and mass flux is 1800kg/m^{2}s.

The case of low mass flux:

Swirl spacer grid > Hybrid spacer grid > V-5H > Two strap spacer grid

The case of high mass flux:

Swirl spacer grid > V-5H > Hybrid spacer grid > Two strap spacer grid

Here, the priority order of spacer grids with four blades was constant. Then, as mass flux, the order of *V-5H* with two split vane is changed and this spacer grid maintains EPR better

than any spacer grid. This is a merit of split vane. It can be applied to the case of 180mm. See Table 3.1.

Another remarkable fact is that the difference of EPR is clearly discrete as mass flux increase. That is, the effect of spacer grid is more and more important as mass flux increase. Maybe it is because the effect on flow structure is dependent on the mass flux.

3.1.3 Spacer Grid Location Effect

In this work it is also investigated that the relationship between the location of spacer grid and CHF enhancement. In previous section, EPR is about 10% at 180mm. On the other hand, when the spacer grid is located at 90mm, EPR increases to about 20%. It seems that the spacer grid effect is decayed out along streamline. This decay rate is different as each spacer grid. Specially, in “two-strap spacer grid”, EPR is has no difference between 90mm and 180mm. In the case of 90mm, the relative EPR to any other spacer grid is smaller than that of the case of 180mm. We know this fact, easily, as Figure 3.2-3.4 and Figure 3.5-3.7. And then EPR of *V-5H* is larger than that of “swirl spacer grid”.

Overall, there are many cases that *V-5H* violates a common trend on a priority order. Therefore it is inferred that *V-5H* has a different effect on the CHF enhancement by the side of other spacer grid.

3.2 Hydraulic Characteristics by Spacer Grid and Mixing Vane

3.2.1 Velocity Profiles and Velocity Fluctuations

In this work, it was measured the axial and lateral velocity profiles and rms values of turbulent fluctuation at 1470kg/m^{2}s. Figure 3.8-3.11 shows the results. Having no concern with spacer grid, trends are similar. Axial velocity is small at center point and is large near the center at just downstream. And first, the profile is flat and finally become parabolic line along streamline. In this work, radial velocity is an important parameter. Mixing vane induces the radial velocity and this forms the swirl flow and cross flow. In *V-5H*, radial velocity decrease suddenly at z=30mm. But in other spacer grid, relatively, it decreases slowly. It means that in the case of *V-5H*, an amount of radial flow form cross flow between subchannels.

With the velocity profile, turbulent intensities also were measured by LDV. Turbulent intensity means rms value of turbulent fluctuation. In spite of exceptions, this value almost converges to specific value at z=90.we will concretely discuss to turbulent intensity in the next section, especially, at a center and gap points.

3.2.2 Estimation Factors

From the previous result, we can estimate the factors which effect on CHF. These are swirl flow, cross flow and turbulent mixing. The definitions were represented in section 2.4. In this experiment, since the number of subchannel is only one, cross flow effect was not concerned.

Two definitions are suggested as estimation factors of swirl flow. One is swirl ratio, the other is angular momentum flux ratio. The former is dimensionless integration of lateral velocity and the latter means the ratio of angular momentum flux and axial momentum flux. And we assumed that swirl flow is circular. Therefore swirl magnitude can be calculated from velocity profile at points along one line. Fig. 3.12-3.13 show swirl magnitude. The priority

order is different as distance from the end of vane blade according to distance and *hybrid spacer grid* has a largest swirl ratio close to spacer grid and *swirl spacer grid* is next. But at the position far away from mixing vane, that is, z=110mm, the order is reversed. In an angular momentum flux ratio, the trend is almost same as that of swirl ratio. The differences are that reversed position move to z=50mm and that in *V-5H*, this factor is better than that of swirl ratio.

In Chapter 2.4, area averaged turbulent kinetic energy ratio is proposed for turbulent mixing. But it is impossible to estimate the factor due to sectional measurement. Therefore, we discuss the turbulent intensity at center and gaps. The position of gap is $z = \pm 5$. From Fig. 4.14, sudden decay of local turbulent energy occurs at regions from 30mm to 60mm. And after this region, there is almost no difference of local turbulent energy.

3.2.3 Pressure Drop

In water test loop, pressure drops are measured. Pressure tabs are at 50mm upward and downward from spacer grid. From Fig. 4.15, though strap length of *hybrid spacer grid* is longer than any other, *hybrid spacer grid* has the smallest pressure drop but *two-strap spacer grid* has the largest. *Swirl spacer grid* is also a good design from the viewpoints of pressure drop. From these results, a blockage area is an important parameter on pressure drop. In *V-5H* or *two-strap spacer grid*, a blockage area is large, relatively.

4. Conclusions

The effects of various spacer grids on CHF have been experimentally investigated in this work on 2*2 rod bundle with R-134a and at the same time, Flow structure and pressure drop by various spacer grid have been also measured and estimated in water loop using LDV. The main conclusions are summarized as follows:

1. Spacer grid enhances CHF and EPRs are about 10% at 180mm and 20% at 90mm. That is, as spacer grid locates far away from the position of CHF occurrence, the effect of spacer grid on CHF is reduced. But the differences of EPR between various spacer grids are clear at high mass flux. Overall, EPR of *swirl spacer grid* is larger than any others. But at high mass flux, *V-5H* may have the largest EPR because EPR of V-5H changed relatively small according to mass flux
2. In water experiment, represented as swirl ratio and angular momentum flux ratio, swirl magnitude is relatively large in cases of *hybrid spacer grid* and *swirl spacer grid*. And line averaged turbulent energies of s*wirl spacer grid* and *hybrid spacer grid* are larger than two others. Therefore, we know that the swirl magnitude and turbulent level are more or less effective to CHF enhancement in a subchannel except *V-5H*. In case of *V-5H*, we need to consider other flow characteristics like cross flow.
3. Pressure drop is different according to spring and dimple shape, strap length, a blockage area and etc. Specially, a blockage area is an important parameter.

Reference	Geometry	Spacer details	Flow conditions	Observed effect
Becker 1964	7-rod	Grid spacers	P=3MPa Xexit=0.1-0.5 G=0.1-0.9 kg/m^2s	Low flow tests, CHF increase by 4%
Rosal 1974	4*4 square	Grid-spacer with and without mixing vanes	P=10-16.5MPa, G=1.4-5.360 Mg/m^2s Subcooled inlet	Mixing vane grids gave highest CHF, up to 26% higher than bundles not equipped with grid spacers.
Guo,Z.C. 1989	4*4 square	Spacer grid and mixing vane	G=1.7Mg/m2s, X_{exit}=-0.15~0.1	Spacer grid location & mixing vane
De Crecy 1994	5*5 square	With mixing vane or without mixing vane	P_{exit}=8.1-17.2 Mpa G=0.98-5.59Mg/m^2s X_{exit} =-0.287~0.355	With mixing vanes, DNB occur on any of rods and is distributed in an apparently random
Cheng,X. 1998	7-rod	Grid spacer, wire wrap	R-12, P=1.0-3.0 Mpa G=1.0-6.0Mg/m^2s Subcooled inlet	The effect of wire wraps on CHF is mainly dependent on local vapour qualities and subsequently on flow regimes

Table 1.1 Previous works of the effects of the spacer grid on the CHF

Name	Mixing Vane	Spring Type	Characteristics
Vantage-5H (No.1)	Split vane	Diagonal spring	
Two strap spacer grid (No.2)	Swirl vane	Plate spring	Nozzle under each blade
Hybrid spacer grid (No.3)	Two different and long vane	H-spring	Height is higher than other grids
Swirl spacer grid (No.4)	Swirl vane	Plate spring	

Table 2.1 Test spacer grids

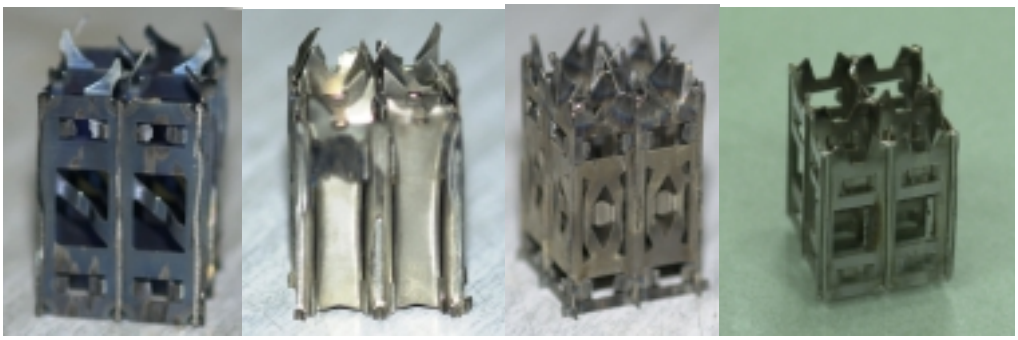

Fig.2.1 Test Spacer Grid (a) V-5H (b) Two-strap (c) Hybrid (d) Swirl

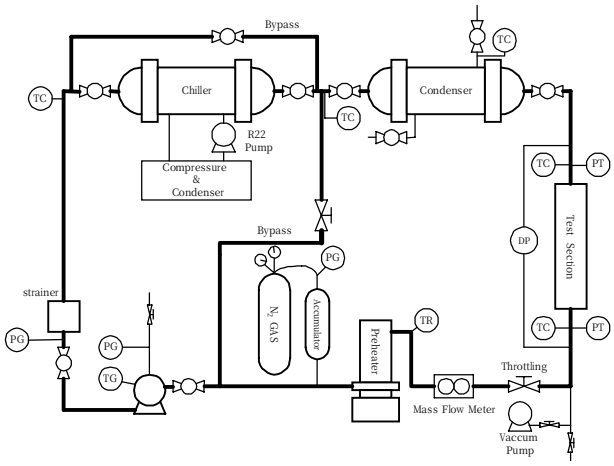

Fig. 2.2 CHF test loop

Pressure [bar]	15 (92.23 bar)	20 (119.8 bar)	25 (146.85 bar)
T_{sat} [^{o}C]	55.24	67.36	77.5
Inlet Temp. [^{o}C]	15	10,15,20	15
Mass Flux [kg/m^{2}s]	1000(*1.06)	1000,1400,1800(*1.2)	1000(*1.61)
# of data	1 point	9 points	1 point

Table 2.2 Test matrix

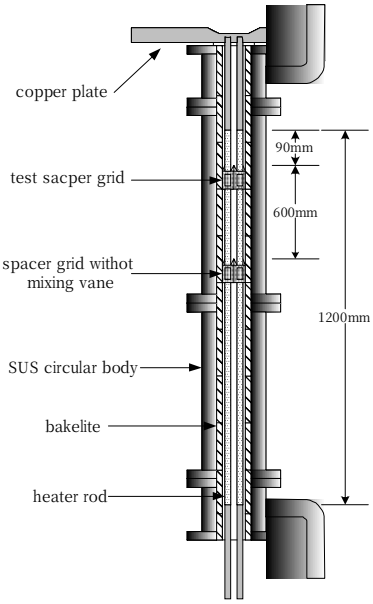

Fig. 2.3 Test section

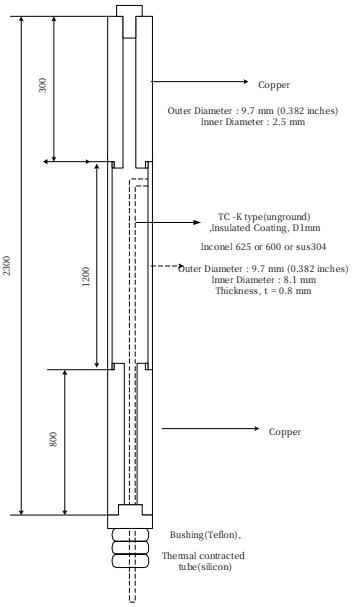

Fig. 2.4 Heater rod

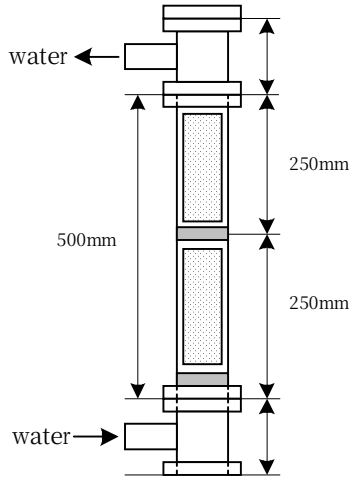

Fig. 2.5 LDV test section

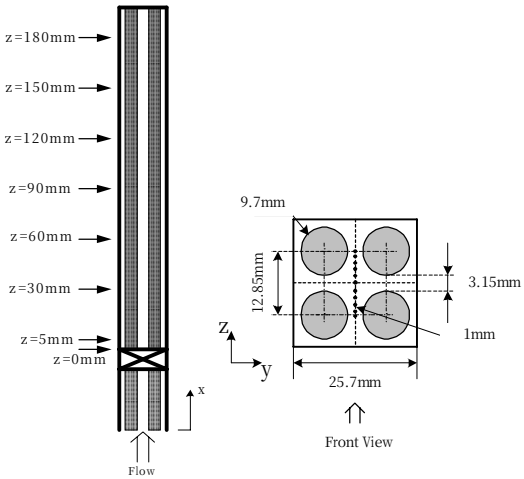

Fig.2.6 Measured locations of axial direction

&

Fig.2.7 Measured points at a cross section

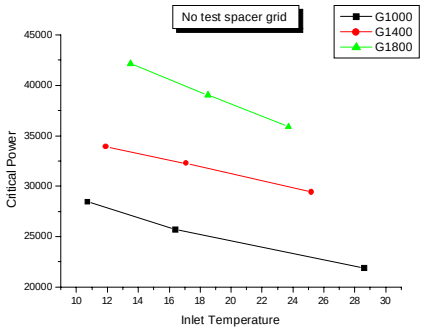

Fig. 3.1 CHF results without spacer grid

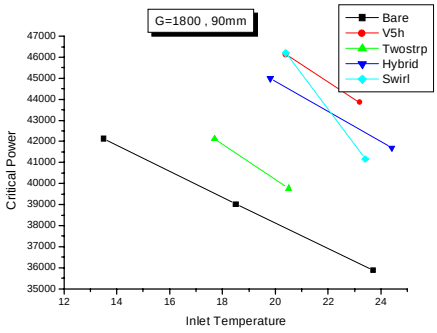

Fig. 3.4 CHF results with spacer grid at 90mm and 1800 kg/m^{2}s

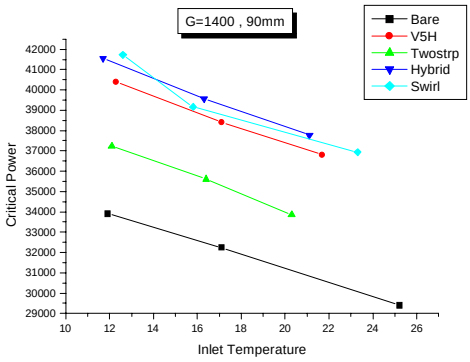

Fig. 3.2 CHF results with spacer grid at 90mm and 1000 kg/m^{2}s

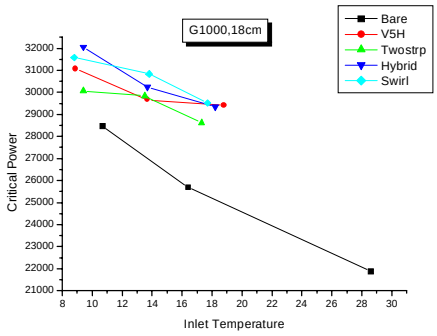

Fig. 3.5 CHF results with spacer grid at 180mm and 1000 kg/m^{2}s

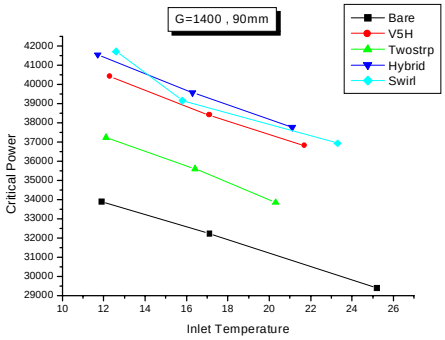

Fig. 3.3 CHF results with spacer grid at 90mm and 1400 kg/m^{2}s

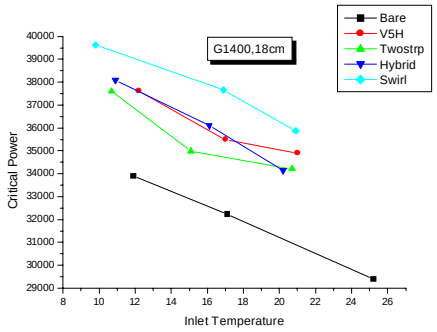

Fig. 3.6 CHF results with spacer grid at 180mm and 1400 kg/m^{2}s

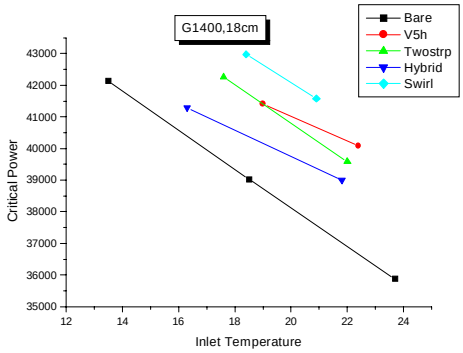

Fig. 3.7 CHF results with spacer grid at 180mm and 1800 kg/m^{2}s

	G=1000	G=1400	G=1800
V-5H	23.05	19.68	21.47
Two Strap	9.91	9.956	5.83
Hybrid	23.79	22.24	17.63
Swirl	25.49	22.2	18.14

Table 3.1 Enhancement Power Ratio at 90mm[%]

	G=1000	G=1400	G=1800
V-5H	11.08	11.44	8.07
Two Strap	8.7	8.79	6.87
Hybrid	12.85	10.53	5.53
Swirl	12.58	15.62	10.24

Table 3.2 Enhancement Power Ratio at 180mm[%]

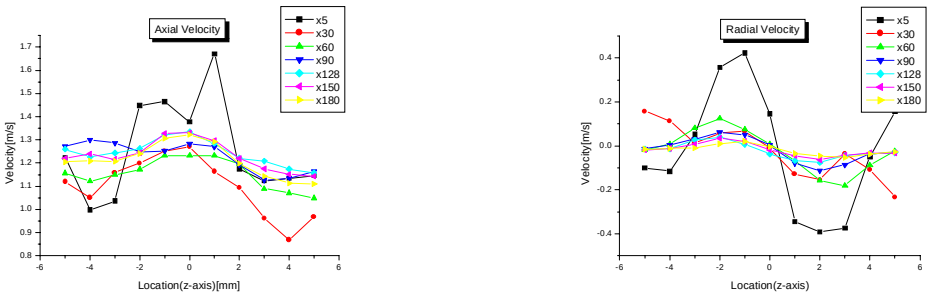

Fig. 3.8 Velocity profiles of No.1

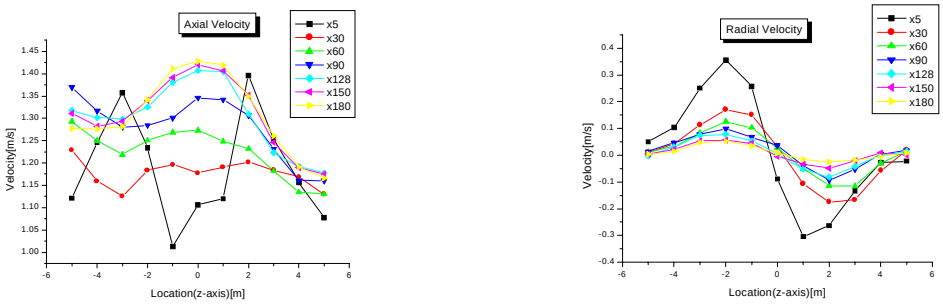

Fig. 3.9 Velocity profiles of No.2

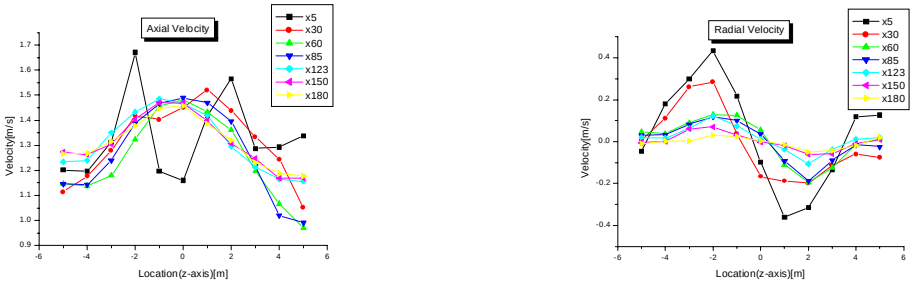

Fig. 3.10 Velocity profiles of No.3

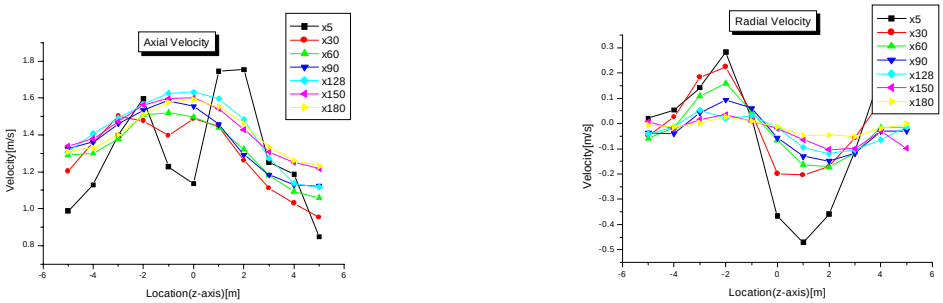

Fig. 3.11 Velocity profiles of No.4

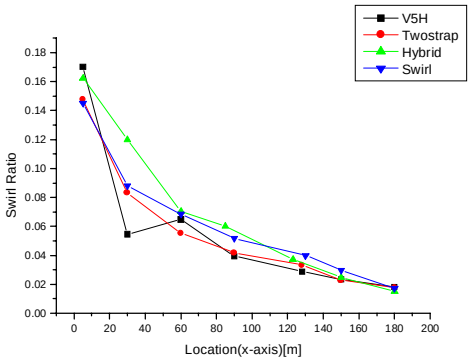

Fig. 3.12 Swirl ratio

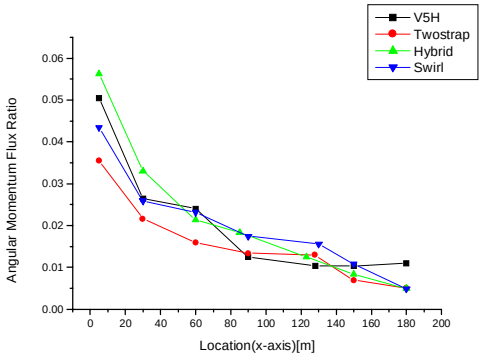

Fig. 3.13 Angular momentum flux ratio

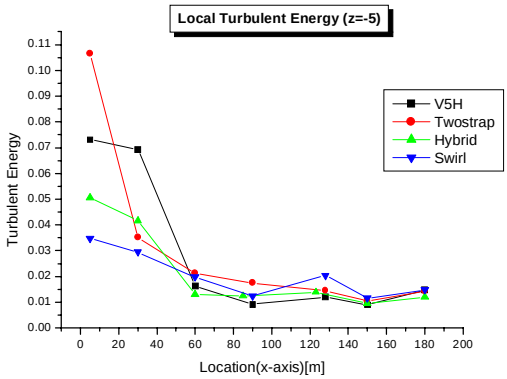

Fig. 3.14(a) Turbulent energy at center

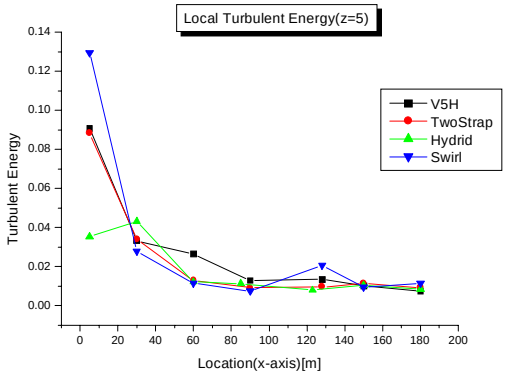

Fig. 3.14(c) Turbulent energy at z=5

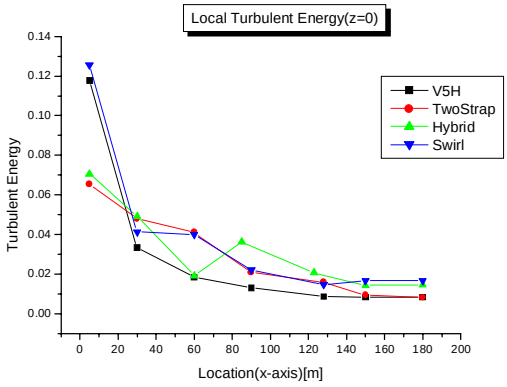

Fig. 3.14(b) Turbulent energy at z=-5

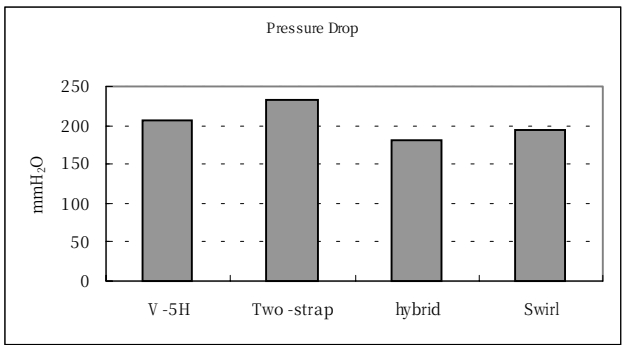

Fig. 3.15 Pressure drop

REFERENCES

[1] ZESES KAROUTAS, CHUN-YUAN GU AND BERTIL SCHOLIN, 3-D FLOW ANALYSES FOR DESIGN OF NUCLEAR FUEL SPACER, NURETH-7, VO1. 4, 1995

[2] YUE FEN SHEN, ZI DONG CAO AND QING GANG LU, AN INVESTIGATION OF CROSSFLOW MIXING EFFECT CAUSED BY GRID SPACER WITH MIXING BLADES IN A ROD BUNDLE, NUCLEAR ENGINEERING AND DESIGN, 1991

[3] SUN KYU YANG AND MOON KI CHUNG, SPACER GRID EFFECTS ON TURBULENT FLOW IN ROD BUNDLES, KNS, VOLUME 28, NUMBER 1, 1996

[4] WANG KEE IN, DONG SEOK OH AND TAE HYUN CHUN, FLOW ANALYSIS FOR OPTIMUM DESIGN OF MIXING VANE IN A PWR FUEL ASSEMBLY, KNS, VOLUME 33, NUMBER 3, PP327~338, 2001

[5] ZORAN STOSIC, ON THE ROLE OF SPACER GRIDS ON CONDITIONS OF DRYOUT/REWETTING AND LOCAL THERMAL HYDRAULICS IN BOILING WATER CHANNELS, NURETH-9, 1999

[6] F. DE CRECY, THE EFFECT OF GRID ASSEMBLY MIXING VANES ON CRITICAL HEAT FLUX VALUES AND AZIMUTHAL LOCATION IN FUEL ASSEMBLIES, NUCLEAR ENGINEERING AND DESIGN, 1994

[7] Z.E. KAROUTAS, P.F. JOFFRE AND L. NORDSTRY, CRITICAL HEAT FLUX TESTING FOR 6*6 ROD BUNDLE GEOMETRY, ICONE,1998

[8] E.R. ROSAL ET AL, HIGH PRESSURE ROD BUNDLE DNB DATA WITH AXIALLY NON-UNIFORM HEAT FLUX, NUCLEAR ENGINEERING AND DESIGN, 1974

[9] J. WEISMAN AND B.S. PEI, PREDICTION OF CRITICAL HEAT FLUX IN FLOW BOILING AT LOW QUALITIES, INT. JOURNAL OF HEAT AND MASS TRANSFER, 1983

[10] C.H. LEE AND I. MUDAWWAR, A MECHANISTIC CRITICAL HEAT FLUX MODEL FOR SUBCOOLED FLOW BOILING BASED ON LOCAL BURK FLOW CONDITIONS, INT. JOURNAL OF MULTIPHASE FLOW VOL.14, NO.6 PP.711-728, 1988

[11] K. REHME, THE STRUCTURE OF TURBULENT FLOW THROUGH ROD BUNDLES, NUCLEAR ENGINEERING AND DESIGN, 1987

[12] V.VONKA, MEASUREMENT OF SECONDARY FLOW VORTICES IN A ROD BUNDLES, NUCLEAR ENGINEERING AND DESIGN,1988